Single-Crystal Optical Actuation Generated by 100% SO2 Linkage Photoisomerization in a Ruthenium-Based Coordination Complex

Jacqueline M. Cole, David J. Gosztola, Jose de J. Velazquez-Garcia, SuYin Grass Wang, and Yu-Sheng Chen

Published version information

Citation: JM Cole et al. Single-Crystal Optical Actuation Generated by 100% SO2 Linkage Photoisomerization in a Ruthenium-Based Coordination Complex. J Phys Chem C 125, no. 36 (2021): 20059-20066

DOI: 10.1021/acs.jpcc.1c05903

Single-crystal Optical Actuation Generated by 100% SO_2 Linkage Photoisomerization in a Ruthenium-based Coordination Complex

Jacqueline M. Cole[1,2,3,4*], David J. Gosztola[4], Jose de J. Velazquez-Garcia[1], SuYin Grass Wang[5], Yu-Sheng Chen[5]

[1]Cavendish Laboratory, Department of Physics, University of Cambridge, J. J. Thomson Avenue, Cambridge, CB3 0HE, UK.

[2]ISIS Neutron and Muon Source, STFC Rutherford Appleton Laboratory, Harwell Science and Innovation Campus, Didcot, OX11 0QX, UK.

[3]Department of Chemical Engineering and Biotechnology, University of Cambridge, West Cambridge Site, Philippa Fawcett Drive, Cambridge, CB3 0AS, UK.

[4]Center for Nanoscale Materials, Argonne National Laboratory, 9700 S Cass Avenue, Argonne, IL 60439, United States.

[5]NSF's ChemMatCARS Beamline, The University of Chicago, Advanced Photon Source, Argonne, IL 60439, United States.

*Correspondence to: jmc61@cam.ac.uk

ABSTRACT

Single-crystal optical actuators are emerging as a new field of materials chemistry owing to their wide-ranging potential applications, from light-induced molecular motors to photo-sensing technologies. Ruthenium-based coordination complexes that contain sulfur dioxide linkage photoisomers have shown particular promise as optical actuators, given that they may exhibit either optical switching or nanooptomechanical transduction in their single-crystal form. The type of single-crystal optical actuation observed in a specific compound within this family of complexes depends upon the nature of the ligand that lies *trans* to this SO_2 linkage photoisomer, since this governs the type and extent of photoisomer (η^2-(OS)O or η^1-OSO) that will form upon the application of light. We report the discovery of a new complex, $[Ru(SO_2)(NH_3)_4$(3-iodopyridine)]tosylate$_2$ (**1**), which forms an η^1-OSO photoisomer with 100% photoconversion upon the application of 505 nm light. The photoisomerization process in the ruthenium-based cation of **1** stimulates rotation and translation of the toluenic constituent of its neighboring anion, thereby affording nanooptomechnical transduction. We show that this η^1-OSO photoisomer transitions to its more thermally stable η^2-(OS)O photoisomer with an activation energy, E_a, of 11(2) kJ/mol, using thermally-activated single-crystal optical absorption spectroscopy. The application of external light

with different wavelengths to **1** is also shown to cause a variation in its optical absorption spectral characteristics. This suggests that the photophysical properties of **1** may be tunable with light.

INTRODUCTION

The growing number of discoveries of new single-crystal optical actuators has stemmed an emerging field of materials chemistry, given their attractive solid-state switching and transduction capabilities,[1-5] which afford them wide-ranging applications: from light-driven molecular rotors,[6] photocatalysis,[7] optical sensing,[8] to futuristic circuitry for quantum computers.[9] Coordination complexes that behave as single-crystal optical actuators via linkage photoisomerization are of particular interest since their metal core provides them with good thermal stability, which is a prerequisite for photonic applications.

Linkage photoisomerization has been discovered in a range of coordination complexes.[10-12] In particular, N_2, NO, NO_2 and SO_2 linkage photoisomers have been identified in certain Group 8 and Group 10 complexes,[11-39] using *in situ* light-induced single-crystal X-ray diffraction, which has become known as photocrystallography.[40-43] "Seeing is believing" with these light-induced crystal structures. Such structures also reveal that the linkage isomers in them do not fully photoconvert, except in a few cases;[35] and the precise photoconversion fraction that is realized in them varies massively from compound to compound, with subtle structural differences often causing major impact on photoconversion levels. Furthermore, the photoconversion fraction achieved is often less than 50%, such that the dark-state linkage isomer remains the dominant species within the overarching 'light-induced' crystal structure. These fractional photoconversion levels somewhat limit the prospective applications of these single-crystal optical actuators.

Most of these examples of single-crystal linkage photoisomerization display optical switching, whereby the dark- and light-induced states represent a 0 and 1. Nanooptomechanical transduction can also occur, even though it is a much rarer type of single-crystal optical actuation. A chemical is a nanooptomechanical transducer if it undergoes a light-driven switching process in which one molecule or ion stimulates mechanical motion in a neighboring molecule or ion. Certain members of a ruthenium sulfur dioxide-based (hereafter [$RuSO_2$]) family of complexes offer some of these rare exceptions.[29-31,35,39] Thereby, nanooptomechanical transduction is achieved by SO_2 linkage photoisomerization in a ruthenium-based cation which, in turn, stimulates mechanical motion in a neighboring anion. This series of complexes possess the generic formula, *trans*-$[Ru(SO_2)(NH_3)_4X]^{m+}Y_n$, whose ligand, X, lies *trans* to the SO_2 ligand, while Y is a counter ion; m and n are integers that refer to charge-balancing requirements, depending on the nature of X and Y. Only certain combinations of X and Y will afford nanooptomechanical transduction, the first example of which was reported by Sylvester and Cole, where X = 3-chloropyridine and Y_n =

tosylate$_2$ or chlorobenzenesulfonate$_2$.[29] S-bound η^1-SO_2 ligands in the dark-state crystal structures of these complexes photoisomerize into O-bound η^1-OSO photoisomers, with a more minor component of a side-bound η^2-(OS)O photoisomer also forming. The non-coordinated oxygen of the η^1-OSO photoisomer within the ruthenium-based cation points towards the arene ring of one of the anions, to which it is so close that the arene ring rotates in order to alleviate crystal-lattice strain (Scheme 1a). Thus, a small mechanical change (SO_2 photoisomerization in the cation) photostimulates a much larger mechanical motion (the arene ring in the anion). These findings by Sylvester and Cole[29] led to the subsequent discovery of several more nanooptomechanical transducers in this family of complexes; [30,31,35,39] one of them, [Ru(SO_2)(NH_3)$_4$(3-bromopyridine)]tosylate$_2$, has been found to exhibit nanooptomechanical transduction with 100% η^1-OSO photoisomer formation.[35] The discovery of this completely photoconverted species is important since it opens up real-world opportunities for these complexes in solid-state optical applications where clean photoswitching is a prerequisite for many photonic device technologies.

This work reports the discovery of *trans*-[Ru(SO_2)(NH_3)$_4$(3-iodopyridine)]tosylate$_2$ (**1**) (Scheme1b) which also turns out to exhibit nanooptomechanical transduction, with 100% photoconversion of its dark-state SO_2 ligands into an η^1-OSO photoisomeric configuration. We will show that the toluenic constituent of one anion in **1** features both rotation and translation as a consequence of SO_2 linkage photoisomerization. While rotation of the arene ring has been observed in the anion of other complexes in this series of [RuSO_2] compounds, the accompanying translational slip of the arene ring from the dark-state configuration that is observed in **1** is unprecedented. We will reason that this more extensive form of nanooptomechanical transduction appears to result from the positional disorder of the iodo substituent that occurs in the cation of both the dark- and light-induced state of **1**. We find that this η^1-OSO photoisomer thermally transitions to its more stable η^2-(OS)O photoisomer, in common with all other η^1-OSO photoisomers that form in this series of [RuSO_2] complexes. We will deduce that this transition proceeds with an activation energy, E_a, of 11(2) kJ/mol, using thermally activated single-crystal optical absorption spectroscopy with a 505 nm externally-applied light source. We will demonstrate that the application of external light to **1** with other wavelengths can cause a variation in its optical absorption spectral characteristics. This suggests that the photophysical properties of **1** may be tunable with light.

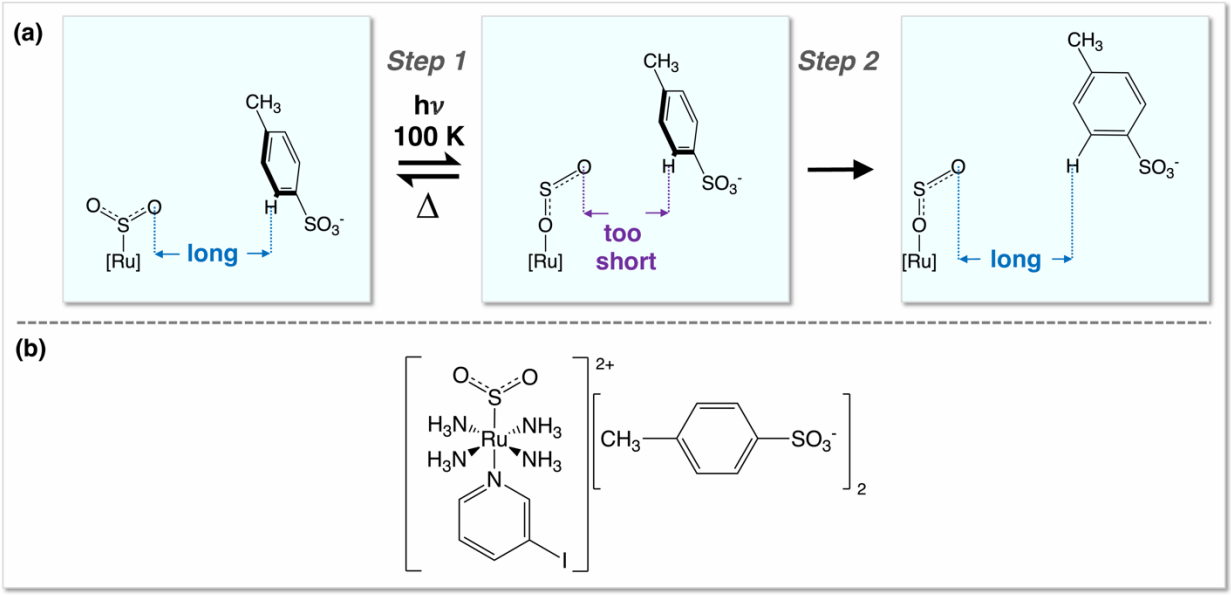

Scheme 1. (a) The operational mechanism of nanooptomechanical transduction for [$RuSO_2$] complexes proposed by Sylvester and Cole.[29] (b) Chemical schematic of **1**.

EXPERIMENTAL METHODS

1 was synthesized from *trans*-[$Ru(SO_2)(NH_3)_4Cl$]Cl, which was synthesized according to a literature procedure.[45] 5 mg (16 □mol) of this precursor in a 500 µL solution of 1 M Na_2CO_3 was mixed with a solution of 3-iodopyridine (12 mg, 59 µmol) in methanol 500 µL. A solution of *p*-tosylic acid (250 µL, 2 M; > 98% purity, Sigma Aldrich) was then added dropwise to this mixture. This produced a precipitate of pale yellow plate-like crystals after 2-4 h at 4 ºC.

Dark and light-induced structures of **1** were characterized by photocrystallography[40-43] at 100 K, using the ChemMatCARS beamline of the Advanced Photon Source, Argonne National Laboratory, IL, USA. Full crystallography details are provided in the Supporting Information; just the relevant photostimulation procedure is given here. Having collected a reference dataset for the dark-state crystal structure of **1**, a 505 nm light-emitting diode (LED) source (ThorLabs M505F3, 1000 mA power output, 3.3 V forward voltage) was used to photostimulate the thinnest face of the 65 x 25 x 10 μm^3 crystal for 2 h. The crystal was then illuminated for an additional 15 mins at three rotated ϕ orientations, 90°, 180° and 270° from its thinnest face, *i.e.* the crystal was photostimulated by 2 hr 45 mins in total for the photocrystallography experiment. This light was switched off before acquiring data for the light-induced crystal structure.

Single-crystal optical absorption spectroscopy was used to determine the photonic properties and thermal stability of **1**. An externally-applied optical pump was employed to stimulate the photoisomerization; thereby, one of four LED sources were applied sequentially with peak

wavelengths of 405 nm (Thorlabs M405F1), 455 nm (Thorlabs M455F3), 505 nm (Thorlabs M505F3) and 530 nm (Thorlabs MF530F2). Spectra were acquired at 100 K, 125 K, 134 K, 138 K, 142 K, 145 K. With the exception of the 100 K option, these correspond to temperatures where the SO_2 ligand in **1** is expected to thermally decay into the side-bound η^2-(OS)O photoisomer, based on results from known nanooptomechanical transducers in the [$RuSO_2$] family of complexes.[29-31] Detailed experimental procedures for these single-crystal optical absorption spectroscopy methods are given by Cole *et al*,[34] while further details specific to **1** are given in the Supporting Information.

RESULTS AND DISCUSSION

Dark-state and light-induced crystal structures of 1

The dark-state and light-induced crystal structures of **1** are displayed in Figures 1a and 1b, respectively. The iodo-substituent exhibits substitutional disorder in both cases, replacing hydrogen on each of the *meta*-pyridyl positions with approximately 50:50 proportioning: 51.4(6):48.6(6)% (dark-state) and 48.6(5):51.4(5)% (light-induced state). Such substitutional disorder is absent in the 3-chloropyridine or 3-bromopyridine crystal-structure analogues, [$Ru(SO_2)(NH_3)_4$(3-halopyridine)]tosylate$_2$ ("halo" = Cl[29] or Br[35]). This stands to reason when one considers the trend in pKa values: 3-chloropyridine (3.31), 3-bromopyridine (3.45), 3-iodopyridine (3.5), i.e. 3-iodopyridine has the highest pKa value which means that it is the weakest π-acceptor of these three ligands but it is strongest σ-donor. The Ru-N_{pyr} coordinative bond in [$Ru(SO_2)(NH_3)_4$(3-halopyridine)]tosylate$_2$ is therefore more prone to free rotation in the case where "halo" = I. Indeed, the 50:50 level of substitutional disorder witnessed in the dark-state and light-induced crystal structures of **1** suggests that there is nothing to hinder free rotation about the Ru-N_{pyr} bond as the cations in **1** assemble during crystallization; free rotation only halts once these cations become confined within the crystal lattice that forms. Once entrapped within this crystal lattice, the iodo species exhibit disorder, presumably because this offers a means by which these large and heavy atoms can fit within the crystal-lattice environment. Achieving such a fit appears to be easier for the iodo substituent that resides on the same side of the cation as per the 3-chloro and 3-bromo crystal-structure analogues.[29,35] Indeed, this 3-iodo species needs to be modeled as two split sites in common with the 3-bromo crystal-structure analogue,[35] although the 3-iodo species will be less susceptible to anion$\cdots\pi$ interactions than its 3-bromo complement[35] since electronegativity of I < Br. Nonetheless, the 3-iodo split component that most protrudes from the pyridyl ring lies over the arene ring in a similar fashion to that observed in [$Ru(SO_2)(NH_3)_4$(3-bromopyridine)]tosylate$_2$,[35] as is illustrated via light-induced crystal structure packing diagram of **1** (Figure 1c).

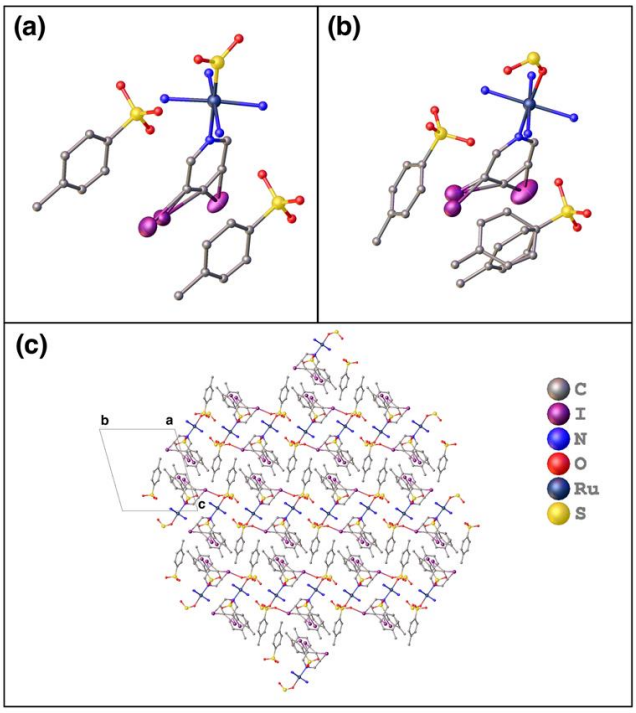

Figure 1 – The (a) dark-state and (b) light-induced crystal structures of **1** as well as its (c) packing diagram as viewed looking down the crystallographic axis, *a*.

The iodo species that resides on the other side of the cation would formally be considered to be a 5-iodo substituent. This is not a position that any other [Ru(SO_2)(NH_3)$_4$(pyridyl ligand)]tosylate$_2$ complex has occupied with any atom except for hydrogen. The unit-cell dimensions of pyridyl-containing [$RuSO_2$] complexes are all very similar, so the presence of such a large and heavy substituent as iodo at the 5-position in its pyridine ligand will mean that it needs to fit within an essentially predefined crystal-lattice environment. In fact, the nature of the disorder refined in **1** shows that the 5-iodo substituent is so hard to place that it is bent inwards to the extent that it is better described as residing between the 4- and 5-position of the pyridine ligand. Even then, this iodo-positioning imposes some crystal-lattice strain on its local environment as is witnessed by the Hirshfeld surface of **1** (see the Supporting Information) which reveals that it makes a very close contact with its neighboring environment.

The entire pyridyl ring is also affected by this iodo disorder, as is manifested by all of its atoms displaying highly elliptical anisotropic displacement parameters (ADPs). This stands to reason given the presence of this disorder and the particularly heavy nature of the iodo substituent. Incidentally, the ADPs of one of the tosylate groups of **1** are also unusually large and elliptical in its dark state. This is the same tosylate anion that is involved in nanooptomechanical transduction in

the light-induced crystal structure of **1**. Thereby, 61(2)% of the toluenic part of this anion rotates and translates in response to 505 nm light, making a dihedral angle of 77(3)° with respect to its dark-state toluenic counterpart (see Figure 1b). This is the highest photoconversion level of any arene ring observed within this family of [$RuSO_2$] complexes. It is also the only crystal structure of a [$RuSO_2$] complex to show both rotation and translation of the arene ring, whereby its motion actually extends to involve the toluenic constituent of the tosylate anion, not just its arene ring. This translational slip may be needed to realize such a high photoconversion level of the arene ring. The substantial disorder observed in the iodo-substituent of the pyridine ligand in **1** may also be a contributory factor in producing either or both of this light-induced translational slip and the particularly high photoconversion level of the toluenic constituent that is observed in this tosylate anion.

Overall, there exists a range of disordered components in the dark-state and light-induced crystal structures of **1**. Indeed, the three zones of crystallographic data manifest this disorder as diffuse scattering, whose features can be related to the direction in which disorder propagates (see Figure 2). Thereby, the dark-state and light-induced crystallographic data of **1** are displayed down their [0kl], [h0l] and [hk0] zones (Figures 2a and 2b) alongside the same viewpoints of the light-induced crystal structure of **1** (Figure 2c). This shows that the diffuse scattering aligns with the disordered features when they are face up in this orientation. For example, the disordered toluenic moiety is face up in the [h0l] zone where the most diffuse scattering is witnessed in the light-induced crystal structure of **1** (Figure 2b, middle), while the level of diffuse scattering is very modest in its dark-state counterpart [h0l] image (Figure 2a, middle). The disorder in the iodo-pyridine ring of **1** is face up in the [0kl] orientation (Figure 2c, top); this disorder exists in both the dark-state and light-induced crystal structure of **1**, so the levels of diffuse scattering in the dark-state and light-induced state crystallographic data are similar (Figure 2a, top; Figure 2b, top). In stark contrast, a negligible level of diffuse scattering is observed, when looking down either the dark-state or light-induced [hk0] crystallographic zone of **1**; this stands to reason because the disorder in **1** lies mostly out of this plane, as illustrated by Figure 2c (bottom). This striking orientation-specific disorder in **1** would also explain our curious observation that many crystals of **1** afforded wholly diffuse diffraction rings that befit an amorphous material when probed with single-crystal X-ray diffraction, despite displaying clearly-defined crystal facets. Moreover, it was much more difficult to crystallize **1** to produce crystals that diffracted suitably well compared with its 3-bromopyridine analogue.[35]

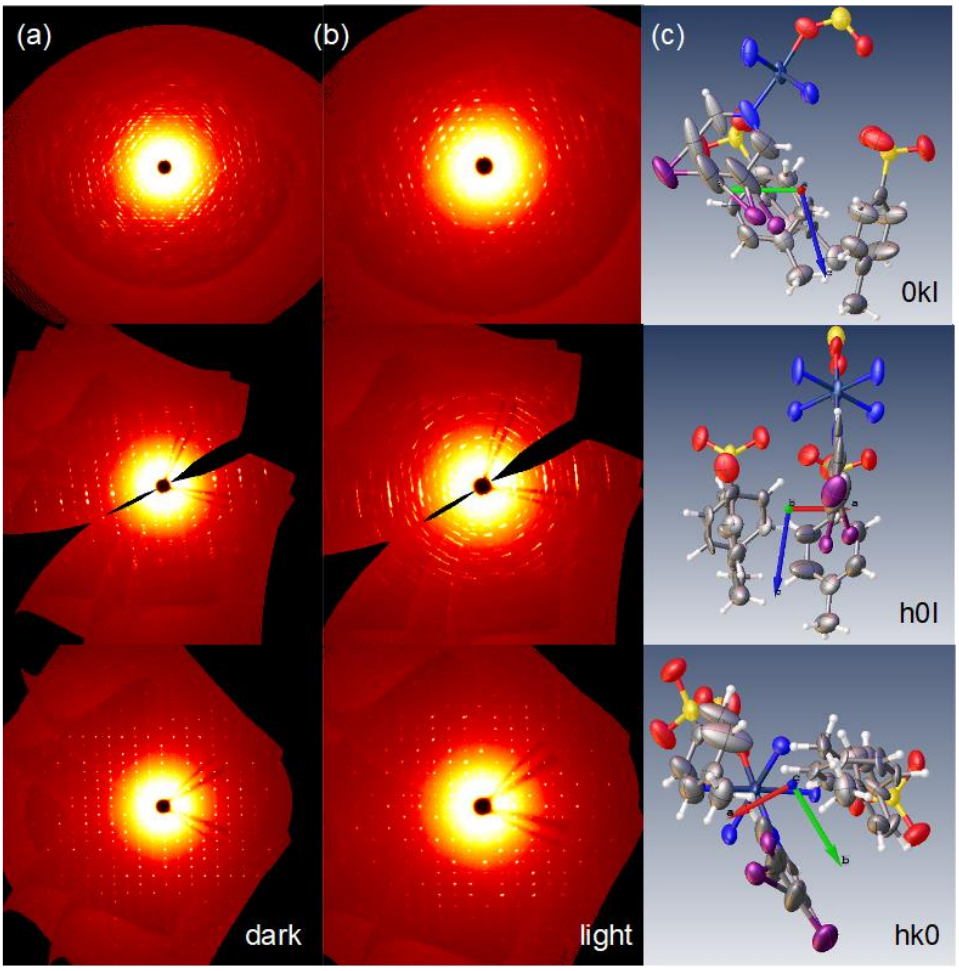

Figure 2 – Crystallographic data, as viewed down the [hk0] (top), [h0l] (middle) and [hk0] (bottom) zones, for the (a) dark-state and (b) light-induced crystal structures of **1**. (c) shows the light-induced crystal structure of **1** oriented along these zone directions.

Single-crystal optical absorption spectra of 1 as a function of photoisomerization time

A single crystal of **1** was subjected to an externally-applied light at 100 K for a sequence of time steps, t, and its single-crystal optical absorption spectrum was measured at each step. This procedure was repeated for four different optical pump wavelengths: 405 nm, 455 nm, 505 nm and 530 nm. The crystal was exposed to a total of 2-3 h of light at each pump wavelength. The results are displayed in Figure 3.

We first consider the series of optical absorption spectra that were acquired using the 505 nm LED source as the optical pump (Figure 3b), since these same light characteristics were used to photoisomerize the crystal in the aforementioned X-ray diffraction experiment.

Light-induced changes in these spectra are initially dominated by the rise of an absorption band in its red region that pertains to the progressive formation of the η^1-OSO photoisomer, in common with what was observed for its 3-bromopyridine analogue.[35] A peak at 625 nm starts to grow on its left shoulder, becoming distinguishable as an individual peak after 2 min of light exposure. Its corresponding absorption band is thought to originate from metal-to-ligand charge transfer (MLCT) that is associated with the pyridyl ligand.[35] This band undergoes solvatochromic shifting until it reaches a maximum optical absorbance at c. 570 nm after 2 h, after which the spectrum remains unchanged, as is verified by the essentially identical spectrum that is revealed after a light-exposure time, t, of 840 min (14 h). Thus, the η^1-OSO photoisomer that has formed in **1** is metastable as long as it remains held at 100 K. Another absorption band also grows in the 400-450 nm region of the spectra, which is thought to be due to the complete loss of the dark-state SO_2 species.[35]

The spectra that were produced using the 455 nm (950 μW) and 530 nm (238 μW) optical-pump wavelengths (power outputs) (Figures 3c and 3d) are very similar to those afforded by the 505 nm LED source (288 μW); even the optical absorbances are similar, despite the much higher power output of the 455 nm source, which suggests that the power provided by the weakest of these sources is already sufficient to maximize the light response of **1**. It stands to reason that they exhibit similar spectral features since their optical pump wavelengths all lie within the bandwidth of the main peak in the dark-state spectrum of **1**. In contrast, spectra that were produced using the 405 nm (265 μW) optical pump wavelength (power output) will photostimulate the lower-wavelength band in the dark-state optical absorption spectrum of **1** that lies within the region c.380-420 nm (Figure 3a). While its spectra appear to be broadly similar to those acquired using 455 nm, 505 nm or 530 nm optical pump wavelengths, there are distinct differences as one might expect. The optical absorbances of all three peaks in Figure 3a are almost equal, with the lowest-wavelength band increasing to less of an extent than when pumped by the other LED sources since this is now the band being pumped. The broad band that is characteristic of η^1-OSO formation shows similar features across all four series of spectra in Figure 3; even the solvatochromic shifting profiles match up in time points, as can be seen by using the t = 2 min spectrum as a marker for each series of spectra since the shifting peak is first discernible at this time point in all four series of spectra. However, this broad band drops off at a distinctly higher wavelength (c.600 nm) when the 405 nm LED source is employed, compared with the c.575 nm peak wavelength drop off that is witnessed in the other three series of spectra shown in Figure 3. Moreover, this drop falls much deeper in the case where the 405 nm optical pump is used, such that the main peak of the dark-state spectrum of **1** is considerably more prominent. This spectral variation makes sense given the different optical pump wavelengths that are employed in relation to the dark-state spectral profile of **1**; it also

suggests that the optical properties of these single-crystal optical actuators may be tunable by the optical pump wavelength, to a certain extent. Further work would be needed to assess if these optical-property modulations may be accompanied by a change in the photoisomerized structural characteristics of **1**; such a prospect has been suggested in recent work on another [$RuSO_2$] complex, owing to similar types of observations.[31]

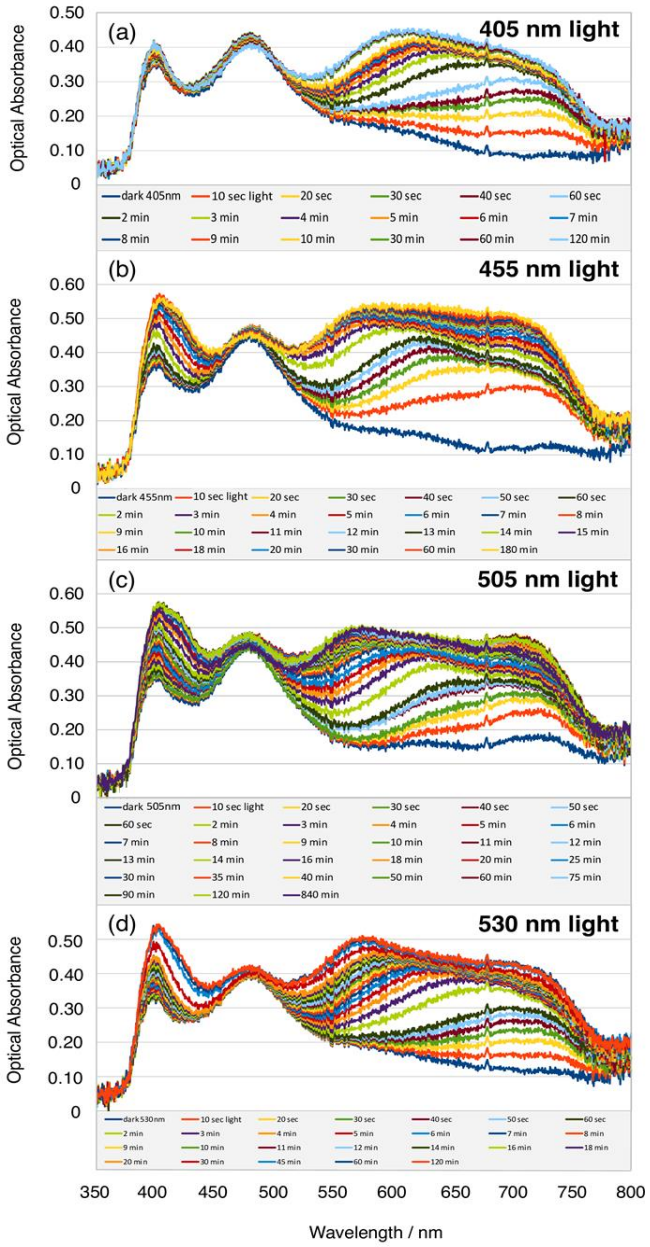

Figure 3 – Single-crystal optical absorption spectra of **1** as a function of light-exposure time using a (a) 405 nm (b) 455 nm (c) 505 nm (d) 530 nm externally-applied LED source.

Thermally-induced η^1-OSO to η^2-(OS)O transition of 1 and its activation energy

Wheresoever an η^1-OSO isomer can be photoinduced within an [$RuSO_2$] complex, it is known to decay into its more thermally-stable η^2-(OS)O photoisomer upon heating a crystal of the complex from 100 K to above a threshold temperature of around 120-130 K, but below the temperature at which the η^2-(OS)O reverts back to its dark-state η^1-SO_2 configuration (of the order of 200 K).[29,30,34,35] The same is true of a crystal of **1**, as is evidenced by five series of single-crystal optical absorption spectra of **1** that were recorded as a function of time lapse, t_l, after having just raised the crystal to one of five temperatures (125 K, 134 K, 138 K, 142 K, 145 K) that lie above the thermal threshold at which it was made metastable by shining 505 nm light onto the crystal for 2 h at 100 K (see Section S3 in the Supporting Information). The thermal decay begins at $t_l = 0$ in all occasions, although this process is naturally slower for a temperature that lies closer to the metastable temperature. This is reflected in the rate constants, k, that were calculated from the associated kinetics data which were extracted from each series of spectra via the following four-step process: (1) the active area under each spectrum (400-775 nm) in Section 3 of the Supporting Information was numerically integrated using the composite Simpson's rule, which is well suited to this task given that there are a large number of finely-spaced data points; (2) the area of the dark-state single-crystal optical absorption spectrum was subsequently subtracted from that of each light-induced spectrum, affording data of the metric, area(light-dark); (3) the order of the photoisomerization process was then determined by exploring the relationship between temperature and the light-driven change in area. Plots of T vs ln(area(light-dark)) afforded linear relationships, revealing that this photoisomerization process displays first-order kinetics; this order-of-reaction assignment is consistent with the findings of previous kinetic experiments on [$RuSO_2$] complexes that used infrared spectroscopy[23,24] or photocrystallography data[29,30,32]; (4) the negative gradient of each T vs ln(area(light-dark)) plot was thus determined, yielding rate constants for the η^1-SO_2 (dark) to η^2-(OS)O (light) photoisomerization process in **1** measured at five temperatures (see Table 1). An associated Arrhenius plot of 1/T versus ln k (Figure 4) afforded an activation energy, E_a, of 11(2) kJ/mol for the thermally-induced η^1-OSO to η^2-(OS)O transition.

Table 1 - First-order rate constants, k, for **1**, derived from a linear fit of elapsed time at the given temperature versus the natural log of the light-induced area of the optical absorption spectrum of **1** at that elapsed time and temperature. R^2 is the coefficient of determination of each linear fit.

Temperature / K (error ± 2.5 K)	Rate constant, k / s^{-1}	Coefficient of determination, R^2
125	3.855×10^{-4}	0.999
134	8.264×10^{-4}	0.995
138	1.540×10^{-3}	0.999
142	1.131×10^{-3}	0.996
145	1.606×10^{-3}	1.000

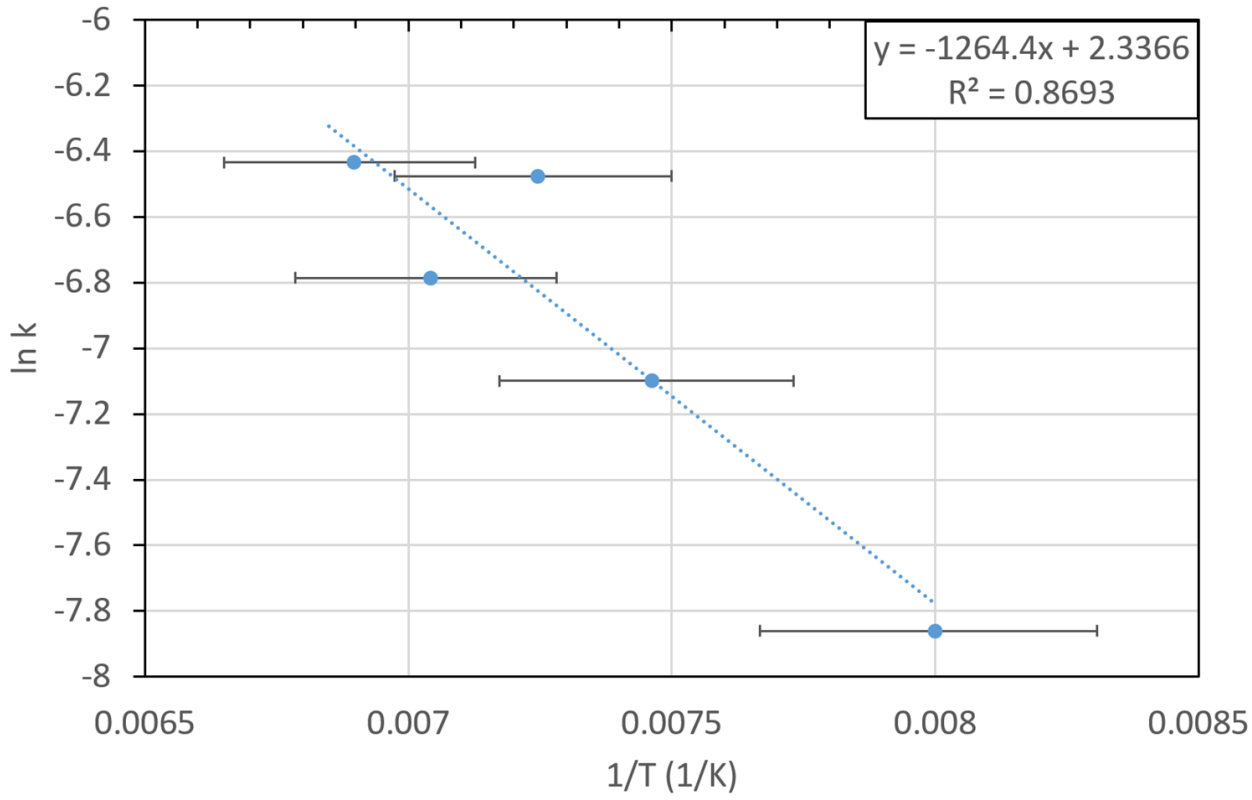

Figure 4 - Arrhenius plot of 1/T versus ln k whose gradient (E_a/R) yields an activation energy, E_a = 11(2) kJ/mol.

This is the first E_a value that has been deduced for such an η^1-OSO to η^2-(OS)O transition in any [$RuSO_2$] complex. Nonetheless, it can be compared with an E_a value for the more thermally-stable η^2-(OS)O to η^1-SO_2 transition that was recently derived for the related complex, [$Ru(SO_2)(NH_3)_4(H_2O)$]tosylate$_2$, using experimental data which afforded E_a = 30(1) kJ/mol. This comparison stands to reason since the η^1-OSO photoisomer is much less thermally stable than the η^2-(OS)O photoisomer. For a broader perspective, the E_a for the η^1-OSO to η^2-(OS)O transition in **1**

can be compared with the typical dissociation energy of a hydrogen bond in the solid state (0.8-167 kJ/mol),[46] *i.e.* the η^1-OSO photoisomer in **1** could be converted into its η^2-(OS)O photoisomer using the energy that it takes to break a weak hydrogen bond. This broader comparison makes it clear how finely tuned an [$RuSO_2$] complex needs to be in order to maintain these SO_2 linkage photoisomers in their metastable state once formed. It also shows how one needs just a subtle change in the crystal structure of a [$RuSO_2$] complex to completely alter its photophysical properties, e.g. whether or not the complex turns out to be a single-crystal nanooptomechanical transducer or just an optical switch. Indeed, very modest changes in the nature of the counterions employed in these [$RuSO_2$] complexes[31] or in their SO_2 reaction cavity topologies[26] have already been shown to cause drastic effects on their optical properties.

CONCLUSIONS

We have reported the discovery of a new single-crystal optical actuator whose functionality stems from SO_2 linkage photoisomerization in the coordination complex, *trans*-[$Ru(SO_2)(NH_3)_4$(3-iodopyridine)]tosylate$_2$ (**1**). The SO_2 ligand transitions from an S-bound η^1-SO_2 isomer to an O-bound η^1-OSO photoisomer with 100 % photoconversion when subjected to 505 nm light. This linkage photoisomerization in the ruthenium-based cation causes the toluenic moiety in a neighboring tosylate anion to rotate and translate, such that the complex undergoes nanooptomechanical transduction. The η^1-OSO photoisomer in **1** thermally decays into a side-bound η^2-(OS)O photoisomer when elevated from 100 K to a temperature in the region of 125-145 K, with an activation energy, E_a, of 11(2) kJ/mol. This low-energy barrier to thermal decay shows that the metastability of an η^1-OSO photoisomer is so finely tuned that an energy as modest as that required to break a weak hydrogen bond is sufficient to overcome it. Indeed, this would explain why only slight changes in the structure of other [$RuSO_2$] complexes that can generate this photoisomer have had drastic effects on their single-crystal optical actuation properties.[31,26] The optical absorption spectral characteristics of **1** have also been found to be somewhat tunable.

ASSOCIATED CONTENT

Supporting Information. Materials characterization methods for **1**; Hirshfeld surface of 1; photochromism of **1** as a function of light exposure time as viewed by single-crystal optical absorption microscopy; single-crystal optical absorption spectra of **1** as a function of thermal decay at five temperatures; crystallographic information files of the dark-state and light-induced state of **1**.

AUTHOR INFORMATION

Corresponding Author

*Email: jmc61@cam.ac.uk (J. M. Cole)

Author contributions

J.M.C. performed all of the photocrystallography, optical microscopy and absorption spectroscopy work, with experimental assistance from D.J.G. in setting up the optical microscopy and absorption spectroscopy apparatus, and S.G.W and Y.-S.C. in beamline operation at the synchrotron. J.M.C carried out the data analysis. J.M.C. was the Ph.D. supervisor of J.dJ.V-G. who synthesized the material. J.M.C. drafted the manuscript. All authors provided input to and agreed on the final manuscript.

Notes

The authors declare no financial conflict of interest.

ACKNOWLEDGMENTS

J.M.C. is grateful for the BASF/Royal Academy of Engineering Research Chair in Data-Driven Molecular Engineering of Functional Materials, which is partly supported by the STFC via the ISIS Neutron and Muon Source. J.M.C. also thanks the 1851 Royal Commission of the Great Exhibition for the 2014 Fellowship in Design, hosted by Argonne National Laboratory where work done was supported by the U.S. Department of Energy (DOE) Office of Science, Office of Basic Energy Sciences, and used research resources of the Center for Nanoscale Materials and the Advanced Photon Source, Office of Science User Facilities operated for the DOE Office of Science by Argonne National Laboratory, supported by the U.S. DOE, all under contract no. DE-AC02-06CH11357. NSF's ChemMatCARS Sector 15 is supported by the Divisions of Chemistry (CHE) and Materials Research (DMR), National Science Foundation, under grant number NSF/CHE-1834750. J.dJ.V-G. acknowledges the National Council of Science and Technology of Mexico (CONACyT) and the Cambridge Trust for a PhD Scholarship (217553).

REFERENCES

1. Naumov, P.; Karothu, D. P.; Ahmed, E.; Catalano, L.; Commins, P.; Halabi, J. M.; Al-Handawi, M. B.; Li, L. The Rise of the Dynamic Crystals. *J. Am. Chem. Soc.* **2020**, *142*, 13256-13272.
2. Naumov, P.; Chizhik, S.; Panda, M. K.; Nath, N. K.; Boldyreva, E. Mechanically Responsive Molecular Crystals. *Chem. Rev.* **2015**, *115*, 12440-12490.
3. Abendroth, J. M.; Bushuyev, O. S.; Weiss, P. S.; Barrett, C. J. Controlling motion at the nanoscale: rise of the molecular machines. *ACS Nano* **2015**, *9*, 7746-7768.
4. Tong, F.; Xu, W.; Guo, T.; Lui, B. F.; Hayward, R. C.; Palffy-Muhoray, P.; Al-Kaysi, R. O.; Bardeen, C. J. Photomechanical molecular crystals and nanowire assemblies based on the

[2+2] photodimerization of a phenylbutadiene derivative. *J. Mater. Chem. C* **2020**, *8*, 5036–5044.

5. Al-Kaysi, R. O.; Tong, F.; Al-Haidar, M.; Zhu, L.; Bardeen, C. J. Highly branched photomechanical crystals. *Chem. Commun.* **2017**, *53*, 2622–2625.
6. Koumura, N.; Zijlstra, R.; van Delden, R.; Harada, N.; Feringa, B. L. Light-driven monodirectional molecular rotor. *Nature* **1999**, *401*, 152-155.
7. Wang, J.; Feringa, B. L. Dynamic Control of Chiral Space in a Catalytic Asymmetric Reaction Using a Molecular Motor. *Science* **2011**, *331*, 1429-1432.
8. Liu, T.; Pagliano, F.; van Veldhoven, R.; Pogoretskiy, V.; Jiao, Y.; Fiore, A. Integrated nano-optomechanical displacement sensor with ultrawide optical bandwidth. *Nat. Commun*. **2020**, *11*, 2407.
9. Bochmann, J.; Vainsencher, A.; Awschalom, D. D.; Cleland, A. N. Nanomechanical coupling between microwave and optical photons. *Nat. Phys.* **2013**, *9*, 712-716.
10. Masciocchi, N.; Kolyshev, A. N.; Dulepov, V. E.; Boldyreva, E. V.; Sironi, A. Study of the Linkage Isomerization $[Co(NH_3)_5NO_2]Br_2 \leftrightarrow [Co(NH_3)_5ONO]Br_2$ in the Solid State by X-ray Powder Diffraction. *Inorg. Chem*. **1994**, *33*, 2579-2585.
11. Coppens, P.; Novozhilova, I.; Kovalevsky, A. Photoinduced Linkage Isomers of Transition-Metal Nitrosyl Compounds and Related Complexes. *Chem. Rev.* **2002**, *102*, 861-883.
12. Hatcher, L. E.; Skelton, J. M.; Warren, M. R.; Raithby, P. R. Photocrystallographic Studies on Transition Metal Nitrito Metastable Linkage Isomers: Manipulating the Metastable State. *Acc. Chem. Res.* **2019**, *52*, 1079-1088.
13. Hatcher, L. E.; Warren, M. R.; Allan, D. R.; Brayshaw, S. K.; Johnson, A. L.; Fuertes, S.; Schiffers, S.; Stevenson, A. J.; Teat, S. J.; Woodall, C. H. *et al.* Metastable Linkage Isomerism in $[Ni(Et_4dien)(NO_2)_2]$: A Combined Thermal and Photocrystallographic Structural Investigation of a Nitro/Nitrito Interconversion. *Angew. Chem., Int. Ed.* **2011**, *50*, 8371-8374.
14. Bajwa, S. E.; Storr, T. E.; Hatcher, L. E.; Williams, T. J.; Baumann, C. G.; Whitwood, A. C.; Allan, D. R.; Teat, S. J.; Raithby, P. R.; Fairlamp, I. J. S. On the appearance of nitrite anion in $[PdX(OAc)L_2]$ and $[Pd(X)(C^{\wedge}N)L]$ syntheses (X = OAc or NO_2): photocrystallographic identification of metastable Pd(η^1-ONO)($C^{\wedge}N$)PPh_3, *Chem. Sci*. **2012**, *3*, 1656-1661.
15. Warren, M. R.; Brayshaw, S. K.; Hatcher, L. E.; Johnson, A. L.; Schiffers, S.; Warren, A. J.; Teat, S. J.; Warren, J. E.; Woodall, C. H.; Raithby, P. R. Photoactivated linkage isomerism in single crystals of nickel, palladium and platinum di-nitro complexes – a photocrystallographic investigation, *Dalton Trans*. **2012**, *41*, 13173-13179.

16. Hatcher, L. E.; Skelton, J. M.; Warren, M. R.; Stubbs, C.; de Silva, E. L.; Raithby, P. R. Monitoring photo-induced population dynamics in metastable linkage isomer crystals: a crystallographic kinetic study of [Pd(Bu$_4$dien)NO$_2$]BPh$_4$, *Phys. Chem. Chem. Phys*. **2018**, *20*, 5874-5886.
17. Hatcher, L. E.; Bigos, E. J.; Bryant, M. J.; MacCready, E. M.; Robinson, T. P.; Saunders, L. K.; Thomas, L. H.; Beavers, C. M.; Teat, S. J.; Christensen, J. *et al*. Thermal and photochemical control of nitro – nitrito linkage isomerism in single-crystals of [Ni(medpt)(NO$_2$)(η^2-ONO)], *CrystEngComm*. **2014**, *16*, 8263-8271.
18. Skelton, J. M.; Crespo-Otero, R.; Hatcher, L. E.; Parker, S. C.; Raithby, P. R.; Walsh, A. Energetics, thermal isomerisation and photochemistry of the linkage-isomer system [Ni(Et$_4$dien)(η^2-O,ON)(η^1-NO$_2$)], *CrystEngComm*, **2015**, *17*, 383-394.
19. Mikhailov, A.; Vukovic, V.; Kijatkin, C.; Wenger, E.; Imlau, M.; Woike, T.; Kostin, G.; Schaniel, D. Combining photoinduced linkage isomerism and nonlinear optical properties in ruthenium nitrosyl complexes, *Acta Crystallogr. B* **2019**, *75*, 1152-1163.
20. Fomitchev, D. V.; Bagley, K. A.; Coppens, P. The First Crystallographic Evidence for Side-On Coordination of N$_2$ to a Single Metal Center in a Photoinduced Metastable State. *J. Am. Chem. Soc.* **2000**, *122*, 532-533.
21. Cheng, L.; Novozhilova, I.; Kim, C. D.; Kovalevsky, A.; Bagley, K. A.; Coppens, P.; Richter-Addo, G. B. First Observation of Photoinduced Nitrosyl Linkage Isomers of Iron Nitrosyl Porphyrins. *J. Am. Chem. Soc.* **2000**, *122*, 7142-7143.
22. Cole, J. M.; Velazquez-Garcia, J. J.; Gosztola, D. J.; Wang, S. G.; Chen, Y.-S. η^2-SO$_2$ Linkage Photoisomer of an Osmium Coordination Complex. *Inorg. Chem.* **2018**, *57*, 2673-2677.
23. Kovalevsky, A. Y.; Bagley, K. A.; Cole, J. M.; Coppens, P. Light-Induced Metastable Linkage Isomers of Ruthenium Sulfur Dioxide Complexes. *Inorg. Chem.* **2003**, *42*, 140-147.
24. Kovalevsky, A. Y.; Bagley, K. A.; Coppens, P. The First Photocrystallographic Evidence for Light-Induced Metastable Linkage Isomers of Ruthenium Sulfur Dioxide Complexes. *J. Am. Chem. Soc.* **2002**, *124*, 9241-9248.
25. Bowes, K. F.; Cole, J. M.; Husheer, S. L. G.; Raithby, P. R.; Savarese, T.; Sparkes, H. A.; Warren, J. E. Photocrystallographic structure determination of a new geometric isomer of [Ru(NH$_3$)$_4$(H$_2$O)(η^1-OSO)][MeC$_6$H$_4$SO$_3$]$_2$. *Chem. Commun.* **2006**, 2448-2450.
26. Phillips, A. E.; Cole, J. M.; d'Almeida, T.; Low, K. S. Effects of the reaction cavity on metastable optical excitation in ruthenium-sulfur dioxide complexes. *Phys. Rev. B* **2010**, *82*, 155118.

27. Sylvester, S. O.; Cole, J. M.; Waddell, P. G. Photoconversion Bonding Mechanism in Ruthenium Sulfur Dioxide Linkage Photoisomers Revealed by in Situ Diffraction. *J. Am. Chem. Soc.* **2012**, *134*, 11860-11863.
28. Phillips, A. E.; Cole, J. M.; d'Almeida, T.; Low, K. S. Ru–OSO Coordination Photogenerated at 100 K in Tetraammineaqua(sulfur dioxide)ruthenium(II) (±)-Camphorsulfonate. *Inorg. Chem.* **2012**, *51*, 1204-1206.
29. Sylvester, S. O.; Cole, J. M. Solar-Powered Nanomechanical Transduction from Crystalline Molecular Rotors. *Adv. Mater.* **2013**, *25*, 3324-3328.
30. Sylvester, S. O.; Cole, J. M.; Waddell, P. G.; Nowell, H.; Wilson, C. SO_2 Phototriggered Crystalline Nanomechanical Transduction of Aromatic Rotors in Tosylates: Rationalization via Photocrystallography of $[Ru(NH_3)_4SO_2X]tosylate_2$ (X = pyridine, 3-Cl-pyridine, 4-Cl-pyridine). *J. Phys. Chem. C* **2014**, *118*, 16003-16010.
31. Cole, J. M.; Gosztola, D. J.; Velazquez-Garcia, J. d. J.; Wang, S. G.; Chen, Y.-S. Rapid build up of nanooptomechanical transduction in single crystals of a ruthenium-based SO_2 linkage photoisomer. *Chem. Commun.* **2021**, *57*, 1320-1323.
32. Sylvester, S. O.; Cole, J. M. Quantifying Crystallographically Independent Optical Switching Dynamics in Ru SO_2 Photoisomers via Lock-and-Key Crystalline Environment. *J. Phys. Chem. Lett.* **2013**, *4*, 3221e3226.
33. Cole, J. M.; Velazquez-Garcia, J. J.; Gosztola, D. J.; Wang, S.-Y. G.; Chen, Y.-S. Light-Induced Macroscopic Peeling of Single-Crystal Driven by Photoisomeric Nano-Optical Switching. *Chem. Mater.* **2019**, *31*, 4927-4935.
34. Cole, J. M.; Gosztola, D. J.; Velazquez-Garcia, J. d. J.; Chen, Y.-S. Systems Approach of Photoisomerization Metrology for Single-Crystal Optical Actuators: A Case Study of $[Ru(SO_2)(NH_3)_4Cl]Cl$. *J. Phys. Chem. C* **2020**, *124*, 51, 28230–28243.
35. Cole, J. M.; Gosztola, D. J.; Velazquez-Garcia, J. d. J. Nanooptomechanical Transduction in a Single Crystal with 100% Photoconversion. *J. Phys. Chem. C* **2021**, *125*, 8907–8915.
36. Cole, J. M.; Gosztola, D. J.; Sylvester, S. O. Low-energy Optical Switching of SO_2 Linkage Isomerisation in Single Crystals of a Ruthenium-based Coordination Complex. *RSC Adv.* **2021**, 11, 13183-13192.
37. Schaniel, D.; Imlau, M.; Weismoeller, M.; Woike, T.; Kraemer, K.; Guedel, H. U. Photoinduced Nitrosyl Linkage Isomers Uncover a Variety of Unconventional Photorefractive Media. *Adv. Mater.* **2007**, *19*, 723-726.
38. Cormary, B.; Ladeira, S.; Jacob, K.; Lacroix, P.; Woike, T.; Schaniel, D.; Malfant, I. Structural Influence on the Photochromic Response of a Series of Ruthenium Mononitrosyl Complexes. *Inorg. Chem.* **2012**, *51*, 7492-7501.

39. Cole, J. M.; Gosztola, D. J.; Sylvester, S. O.; Wang, SY-G.; Chen, Y-S. Assigning Optical Absorption Transitions with Light-Induced Crystal Structures: Case Study of a Single-Crystal Nanooptomechanical Transducer. *J. Phys. Chem. C* **2021**, *125*, 15711–15723.
40. Coppens, P.; Fomitchev, D. V.; Carducci, M. D.; Culp, K. Crystallography of molecular excited states. Transition-metal nitrosyl complexes and the study of transient species. *J. Chem. Soc., Dalton Trans.* **1998**, *6*, 865-872.
41. Cole, J. M. Single-crystal X-ray diffraction studies of photo-induced molecular species. *Chem. Soc. Rev.* **2004**, *33*, 501-513.
42. Cole, J. M. Photocrystallography. *Acta Crystallogr., Sect. A: Found. Crystallogr.* **2008**, *64*, 259-271.
43. Cole, J. M. A new form of analytical chemistry: distinguishing the molecular structure of photo-induced states from ground-states. *Analyst* **2011**, *136*, 448-455.
44. Hatcher, L. E. Raising the (metastable) bar: 100% photo-switching in $[Pd(Bu_4dien)(\eta^1\text{-}NO_2)]^+$ approaches ambient temperature. *Cryst. Eng. Comm.* **2016**, *18*, 4180-4187.
45. Vogt, L. H.; Katz, J. L.; Wiberley, S. E. The Crystal and Molecular Structure of Ruthenium-Sulfur Dioxide Coordination Compounds. I. Chlorotetraammine(sulfur dioxide)ruthenium (II) Chloride. *Inorg. Chem.* **1965**, *4*, 1157–1163.
46. Steiner, T. The Hydrogen Bond in the Solid State. *Angew. Chem., Int. Ed.* **2002**, *41*, 48-76.

TOC Graphic

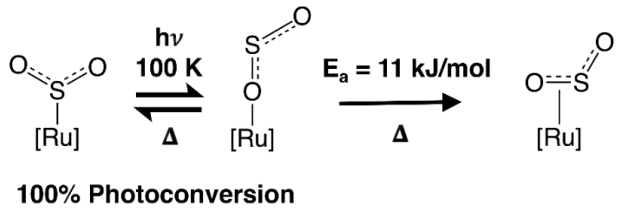

100% Photoconversion

Supporting Information for:

Single-crystal Optical Actuation Generated by 100% SO_2 Linkage Photoisomerization in a Ruthenium-based Coordination Complex

Jacqueline M. Cole[1,2,3,4*], David J. Gosztola[4], Jose de J. Velazquez-Garcia[1], SuYin Grass Wang[5], Yu-Sheng Chen[5]

[1]Cavendish Laboratory, Department of Physics, University of Cambridge, J. J. Thomson Avenue, Cambridge, CB3 0HE, UK.

[2]ISIS Neutron and Muon Source, STFC Rutherford Appleton Laboratory, Harwell Science and Innovation Campus, Didcot, OX11 0QX, UK.

[3]Department of Chemical Engineering and Biotechnology, University of Cambridge, West Cambridge Site, Philippa Fawcett Drive, Cambridge, CB3 0AS, UK.

[4]Center for Nanoscale Materials, Argonne National Laboratory, 9700 S Cass Avenue, Lemont, IL 60439, United States.

[5]NSF's ChemMatCARS Beamline, The University of Chicago, Advanced Photon Source, Lemont, IL 60439, United States.

* Author for correspondence (J. M. Cole): jmc61@cam.ac.uk

Table of Contents

S1 - Materials Characterization Methods for 1

Dark and Photo-induced *In-Situ* Single-Crystal X-ray Diffraction of 1. Dark and light-induced crystal structures of **1** were determined using synchrotron-based X-ray photocrystallography, at the ChemMatCARS beamline of the Advanced Photon Source, Argonne National Laboratory, IL, USA. A 65 x 25 x 10 μm^3 crystal of **1** was mounted onto a Huber three-circle diffractometer equipped with a Pilatus 3 x CdTe 1M shutterless pixel array detector and a 100 K nitrogen open-flow cryostream delivered by an Oxford cryojet. Crystallography data were acquired using a 100 x 100 μm X-ray beam of wavelength 0.41328 Å. For control purposes, the ambient lighting in the experimental hutch of the beamline was extinguished while data were being collected. A reference dataset for the dark-state crystal structure was first obtained. Each crystal was then maintained at 100 K on the diffractometer while 505 nm light was shone onto it for *n* minutes (where *n* = total light exposure time), using a Thorlabs M505L3 light emitting diode (LED) whose head power output was 1000 mA constant current and 3.3 V forward voltage. This light was switched off before acquiring data for each light-induced crystal structure. Further experimental details, as well as structure solution and refinement information, are given in the accompanying Crystallographic Information Files. More technical details of the photocrystallography are given elsewhere.[1-5]

Single crystal optical absorption spectroscopy and microscopy of 1. A custom-built micro-spectroscopy system was used to record the absorption spectra of single crystals under a variety of environmental conditions. The system was built around an inverted microscope (Olympus: IX71) coupled to a 300 mm focal length spectrograph (Princeton Instruments: Acton Series 2300i) and 1320 x 100 channel CCD camera (Princeton Instruments: PIXIS 100BR). A 0.410 x 0.130 x 0.025 μm^3 crystal of **1** was mounted on a sapphire disk (9 mm dia., 0.5 mm thick) and fastened with a small amount of viscous perfluoroether oil. The mounted sample was then placed on the cold finger of an optical cryostat (Janis: ST-500-UC) attached to the microscope. The cold finger was drilled through, allowing optical absorption measurements to be made. The crystal was positioned such that only half of the active vertical channels of the CCD camera were used to image a portion of the crystal using a 5 x, 0.13NA objective (Olympus, NeoSPlan); the remaining half of the active detector channels imaged the sapphire substrate. The probe light for optical absorption measurements was provided by the microscope's 100W tungsten-halogen lamp and 0.3 NA condenser optics. A visible bandpass filter (Schott: BG40) and OD 0.9 neutral density filter was placed between the lamp and the condenser to reduce thermal load on the sample and cryostat.

To induce photoisomerization, the crystal was illuminated with a 405 nm (Thorlabs M405F1), 455 nm (Thorlabs M455F3), 505 nm (Thorlabs M505F3) or 530 nm (Thorlabs MF530F2) fibre optically coupled light-emitting diode (LED). The light from the LED was collimated and then coupled into the microscope through a side port, focusing it onto the back aperture of the objective, thus filling the field of view and evenly illuminating the entire crystal. The excitation power measured at the objective was typically 265 μW, 950 μW, 288 μW, or 238 μW giving an estimated 12 $\mu W/mm^2$, 43 $\mu W/mm^2$, 13 $\mu W/mm^2$ or 11 $\mu W/mm^2$ illuminating the field of view.

Optical absorption spectra were recorded by imaging the crystal on the entrance slit (75 μm) of the spectrometer and dispersing the light, using a 150 line/mm grating, onto the detector. The image was positioned such that 20 rows of the detector were illuminated with light that passed through the crystal (I_T); whereas 20 rows of the detector directly above the crystal recorded light that passed through only the sapphire substrate (I_0). Absorption spectra were calculated as $\log_{10}(I_T/I_0)$.

A more detailed description of this custom instrument set up and its operational pipeline, as provisioned to support photocrystallography, is given elsewhere.[6]

S2 – Hirshfeld surface of 1

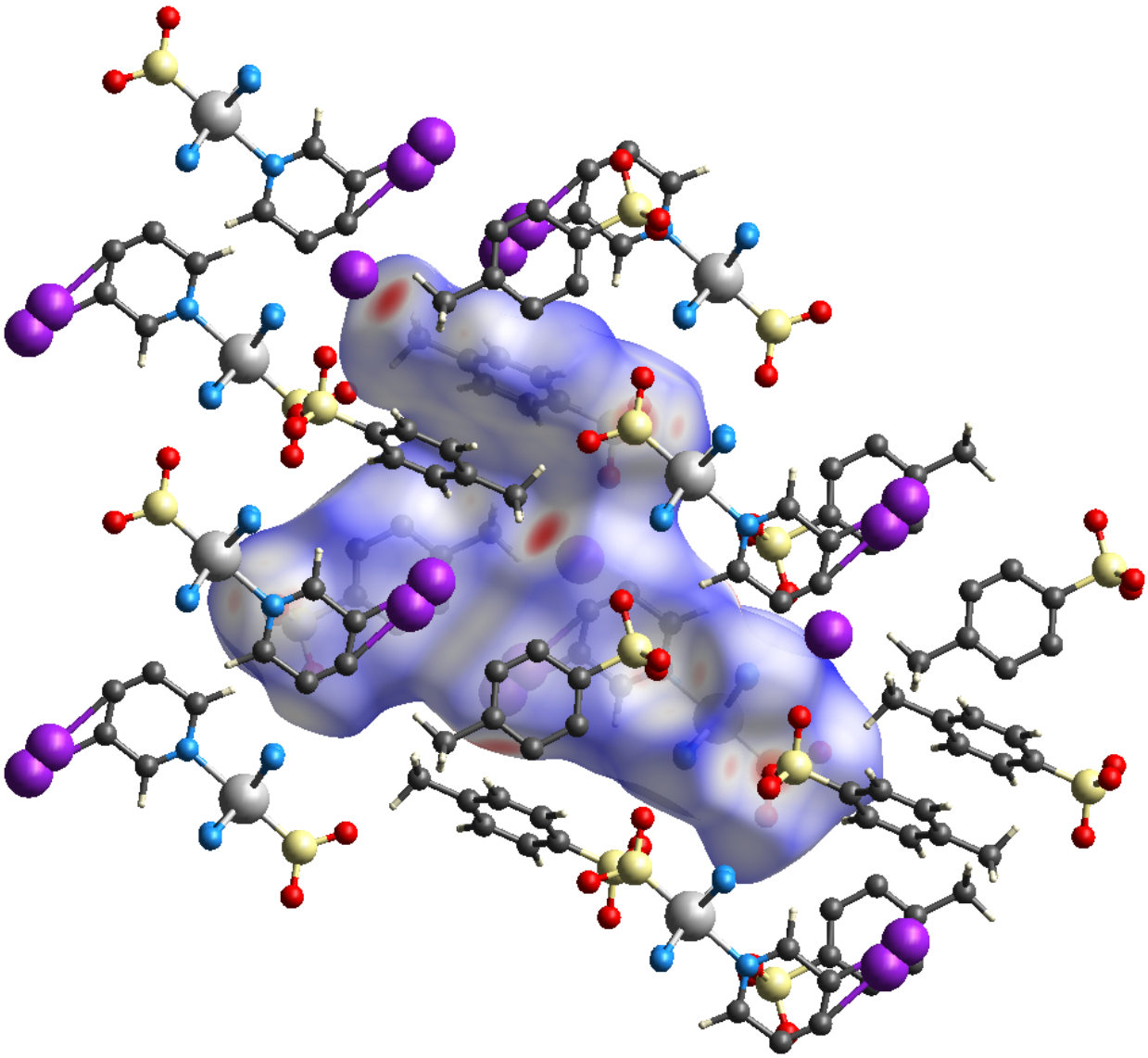

Figure S1 - Hirshfeld surface of **1** showing how the close proximity of the non-split iodo substituent to the methyl group of one of the tosylate ions induces a significant non-bonded contact (in red). The red, white and blue regions show positive, neutral and negative isoenergies. The image was generated via CrystalExplorer.[7]

S3 – Single-crystal optical absorption spectroscopy of 1 as a function of thermal decay at five temperatures

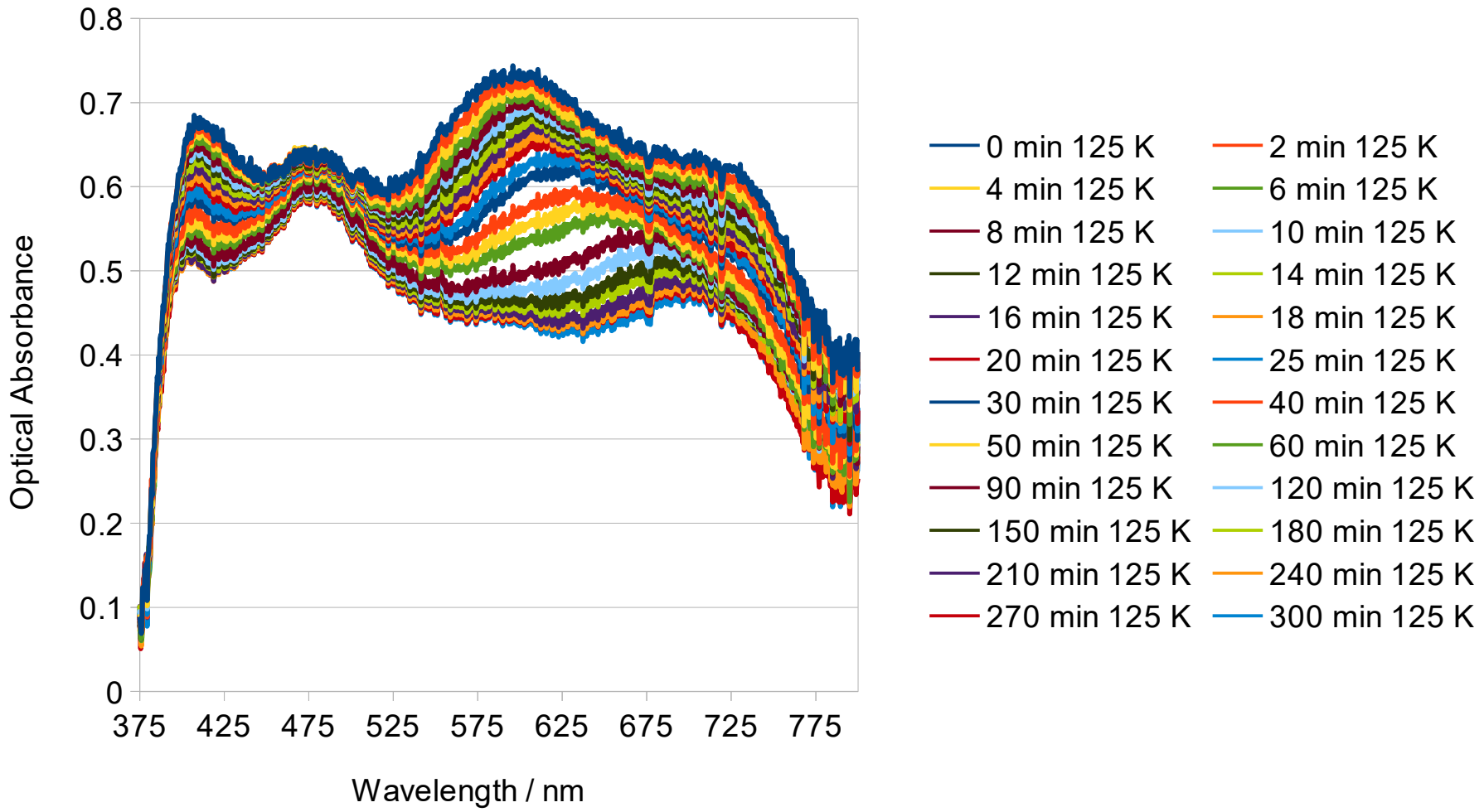

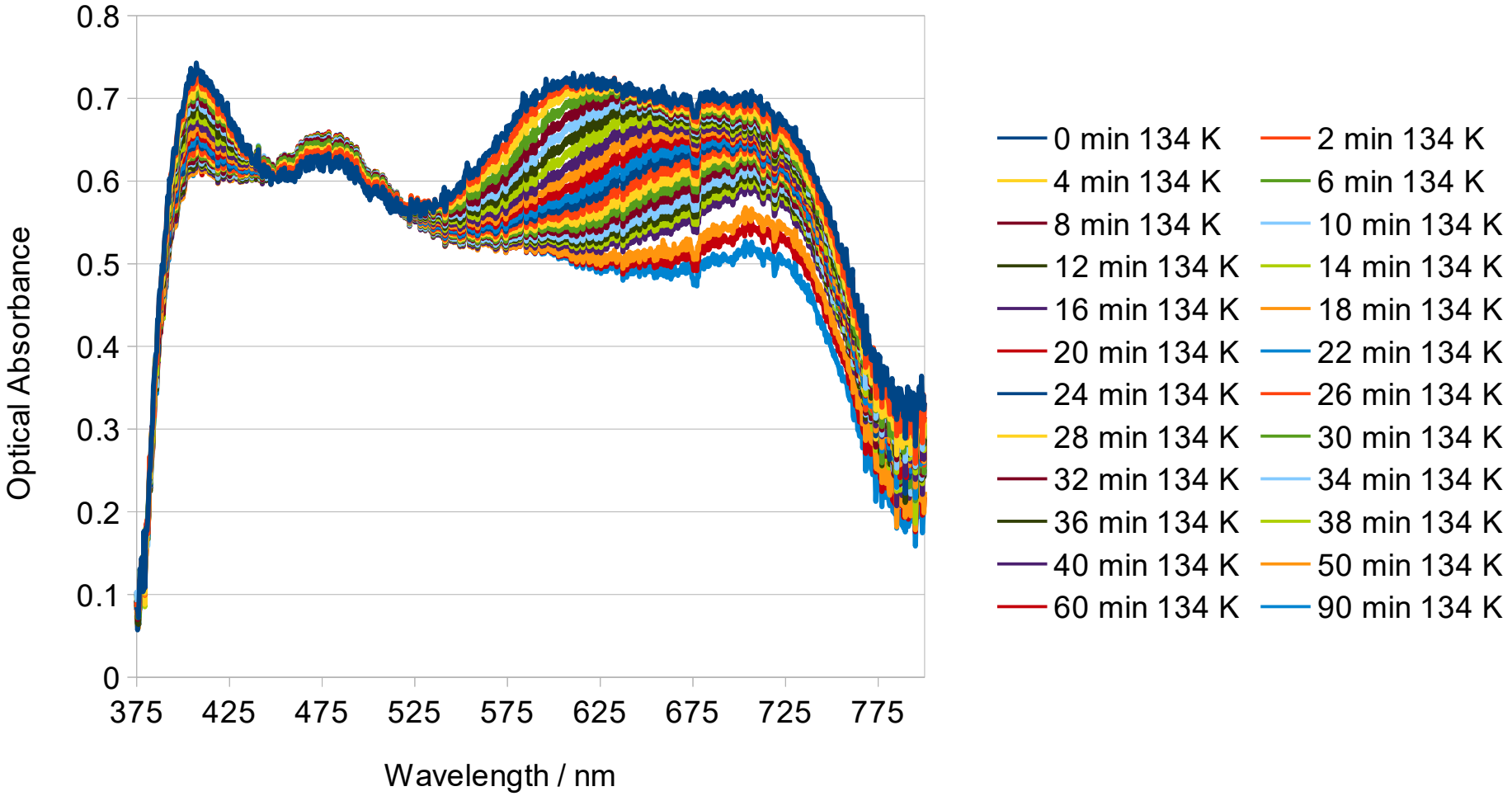
Optical Absorbance
0.8
0.7
0.6
0.5
0.4
0.3
0.2
0.1
0
375
425
475
525
575
625
675
725
775
Wavelength / nm
0 min 134 K
2 min 134 K
4 min 134 K
6 min 134 K
8 min 134 K
10 min 134 K
12 min 134 K
14 min 134 K
16 min 134 K
18 min 134 K
20 min 134 K
22 min 134 K
24 min 134 K
26 min 134 K
28 min 134 K
30 min 134 K
32 min 134 K
34 min 134 K
36 min 134 K
38 min 134 K
40 min 134 K
50 min 134 K
60 min 134 K
90 min 134 K

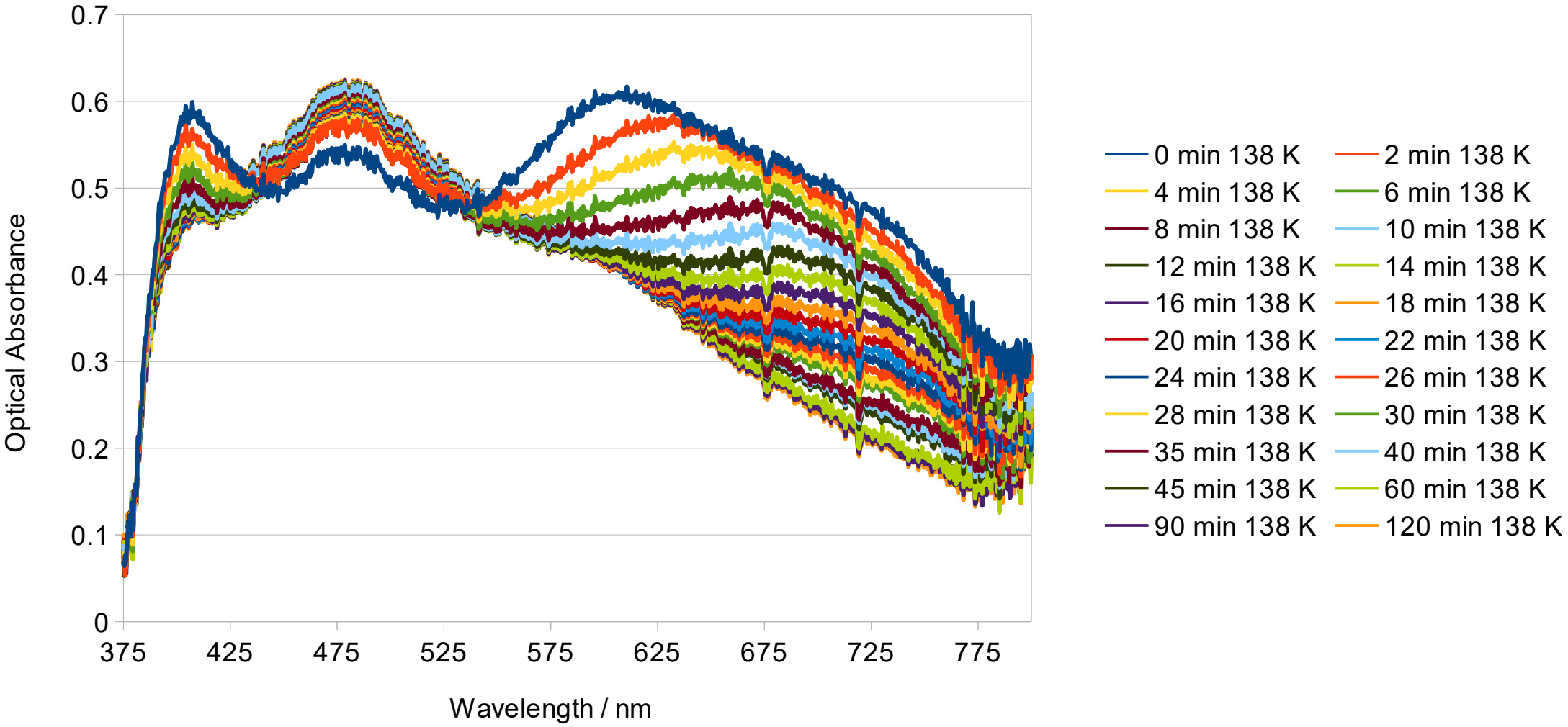
0.7
0.6
0.5
0.4
0.3
0.2
0.1
0
Optical Absorbance
375
425
475
525
575
625
675
725
775
Wavelength / nm
0 min 138 K
2 min 138 K
4 min 138 K
6 min 138 K
8 min 138 K
10 min 138 K
12 min 138 K
14 min 138 K
16 min 138 K
18 min 138 K
20 min 138 K
22 min 138 K
24 min 138 K
26 min 138 K
28 min 138 K
30 min 138 K
35 min 138 K
40 min 138 K
45 min 138 K
60 min 138 K
90 min 138 K
120 min 138 K

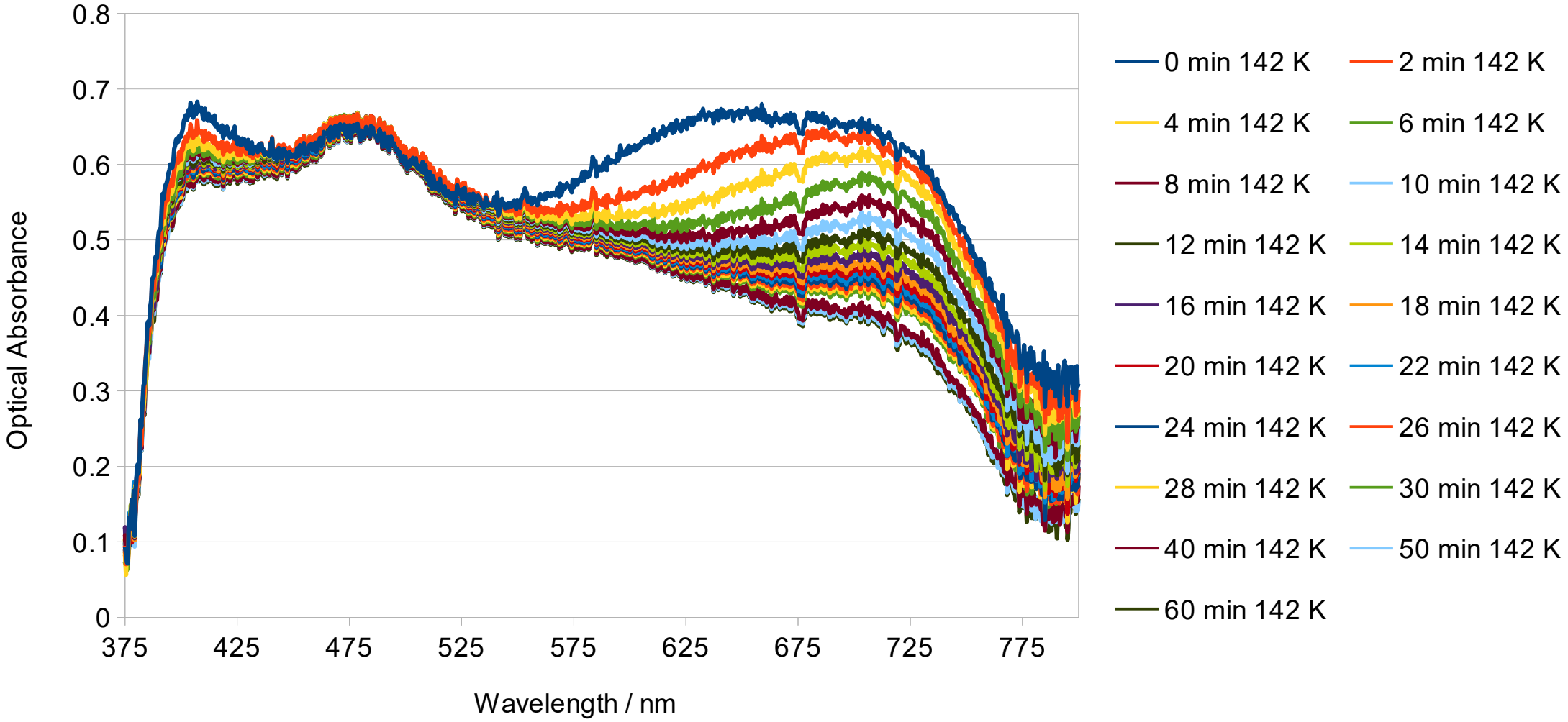
Optical Absorbance
0.8
0.7
0.6
0.5
0.4
0.3
0.2
0.1
0
375
425
475
525
575
625
675
725
775
Wavelength / nm
0 min 142 K
2 min 142 K
4 min 142 K
6 min 142 K
8 min 142 K
10 min 142 K
12 min 142 K
14 min 142 K
16 min 142 K
18 min 142 K
20 min 142 K
22 min 142 K
24 min 142 K
26 min 142 K
28 min 142 K
30 min 142 K
40 min 142 K
50 min 142 K
60 min 142 K

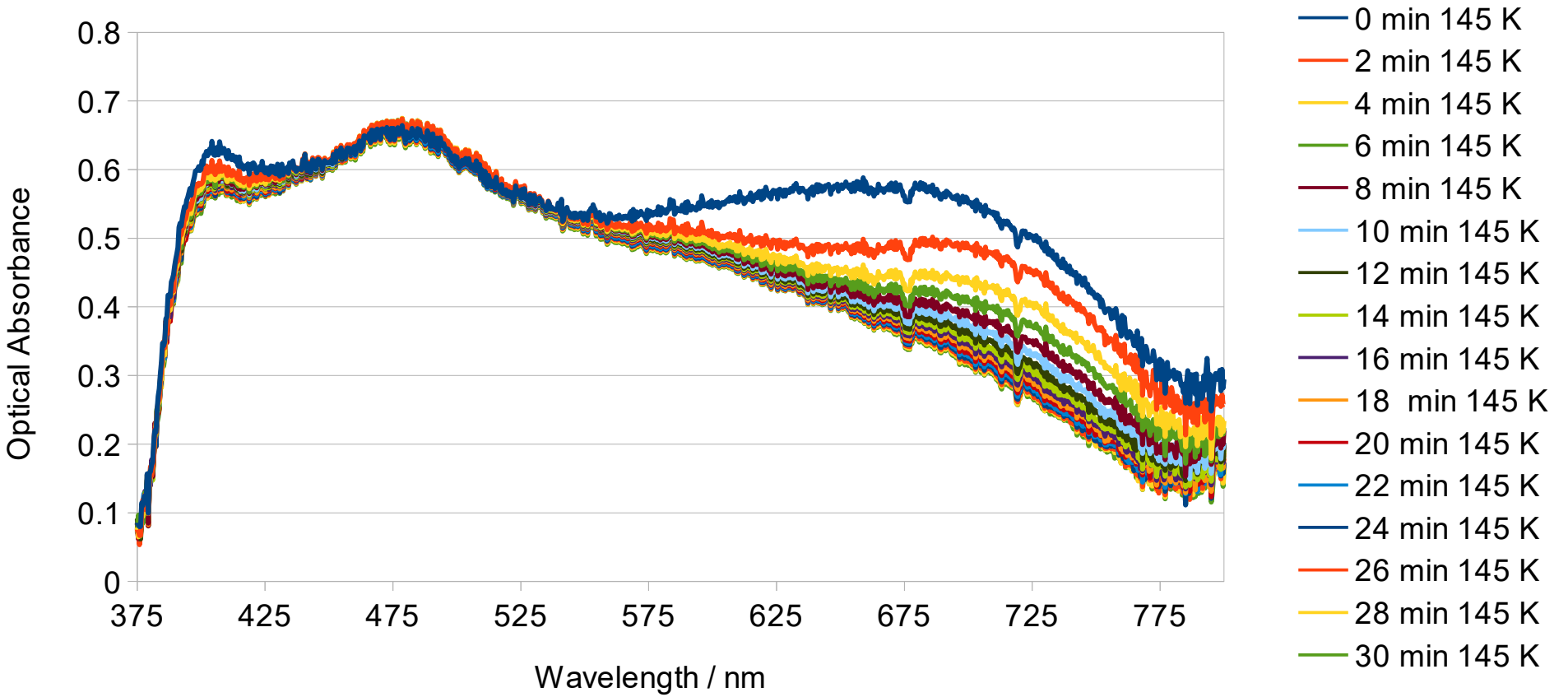
Optical Absorbance
0.8
0.7
0.6
0.5
0.4
0.3
0.2
0.1
0
375
425
475
525
575
625
675
725
775
Wavelength / nm
0 min 145 K
2 min 145 K
4 min 145 K
6 min 145 K
8 min 145 K
10 min 145 K
12 min 145 K
14 min 145 K
16 min 145 K
18 min 145 K
20 min 145 K
22 min 145 K
24 min 145 K
26 min 145 K
28 min 145 K
30 min 145 K

S4 – References

[1] Coppens, P.; Fomitchev, D. V.; Carducci, M. D.; Culp, K. Crystallography of molecular excited states. Transition-metal nitrosyl complexes and the study of transient species. *J. Chem. Soc., Dalton Trans.* **1998**, *6*, 865-872.
[2] Cole, J. M. Single-crystal X-ray diffraction studies of photo-induced molecular species. *Chem. Soc. Rev.* **2004**, *33*, 501-513.
[3] Cole, J. M. Photocrystallography. *Acta Crystallogr., Sect. A: Found. Crystallogr.* **2008**, *64*, 259-271.
[4] Cole, J. M. A new form of analytical chemistry: distinguishing the molecular structure of photo-induced states from ground-states. *Analyst* **2011**, *136*, 448-455.
[5] Cole, J. M., Applications of photocrystallography: a future perspective. *Z. Kristallogr.* **2008**, *223*, 363-369.
[6] Cole, J. M.; Gosztola, D. J.; Velazquez-Garcia, J. J.; Chen, Y-S. Systems Approach of Photoisomerization Metrology for Single-Crystal Optical Actuators: A Case Study of $Ru(SO_2)(NH_3)_4Cl]Cl$. *J. Phys. Chem. C* **2020**, 124, 51, 28230–28243.
[7] Turner, M. J.; McKinnon, J. J.; Wolff, S. K.; Grimwood, D. J.; Spackman, P. R.; Jayatilaka, D.; Spackman, M. A. CrystalExplorer17 (2017). University of Western Australia. https://hirshfeldsurface.net.